Journal of Alloys and Compounds 509 (2011) 1665–1671

Contents lists available at ScienceDirect

Journal of Alloys and Compounds

journal homepage: www.elsevier.com/locate/jallcom

Influence of partial substitution of Ge on crystallization kinetics, microstructure and magnetic property of $Fe_{44}Co_{44-x}Zr_7B_5Ge_x$ alloys

Yao Sun, Xiaofang Bi*

Key Laboratory of Aerospace Materials and Performance (Ministry of Education), School of Materials Science and Engineering, Beijing University of Aeronautics and Astronautics, Beijing 100191, China

ARTICLE INFO

Article history:
Received 24 July 2010
Received in revised form
17 September 2010
Accepted 18 September 2010
Available online 25 September 2010

Keywords:
$Fe_{44}Co_{44-x}Zr_7B_5Ge_x$ alloys
Crystallization kinetics
Microstructure
Magnetic property

ABSTRACT

Partial substitution of Ge for Co in $Fe_{44}Co_{44}Zr_7B_5$ amorphous alloy is found to have a large influence on crystallization kinetics and magnetic property of the alloy. Activation energy of nanocrystallization of FeCo phase (primary crystallization) decreases by 90 kJ/mol with 4 at.% Ge substitution, while that of precipitations of Zr-type phase from a residual amorphous phase (secondary crystallization) increases by 106 kJ/mol. The suppression of the secondary crystallizations stabilizes the FeCo nanocrystals embedded in the residual amorphous phase for the $Fe_{44}Co_{44-x}Zr_7B_5Ge_x$ until higher temperatures. It is proposed that the stabilization mechanism is attributed to preferential partitioning of Ge in the residual amorphous phase revealed by scanning transmission electron microscopy analysis. Microstructure and coercivity for the annealed alloys are also presented in combination with the effect of the Ge substitutions.

1. Introduction

FeCo-based nanocrystalline soft magnetic alloys characterized by FeCo nanocrystals embedded in a residual amorphous matrix have attracted growing attention due to high Curie temperature of the amorphous phase [1,2] which is responsible for retention of magnetic exchange coupling between the nanocrystals up to higher temperatures as compared to Fe-based and FeSi-based nanocrystalline alloys. As temperatures rise above the Curie temperature of the amorphous phase, however, the nanocrystals become exchange-decoupled, resulting in magnetic hardening of the two-phase systems [3,4]. In addition to the intergranular magnetic coupling, nanocrystalline microstructure is another significant contribution to outstanding soft magnetic properties for the alloys. Based on the random anisotropy model, magnetic anisotropy is averaged out over several small grains when nanograin size (D) is smaller than exchange correlation length. Coercivity (H_c) can be greatly reduced with a decrease of nanograin size, following the well-known relationship: $H_c \sim D^{-6}$ [5–7]. This indicates that thermal stability of nanocrystalline microstructure is also a prime factor for remaining excellent soft magnetic properties at high temperatures. Indeed, previous studies have found that magnetic hardening occurs around secondary crystallization temperatures for FeCo-based alloy, although its residual amorphous phase still exhibits ferromagnetic characters [8,9]. The deterioration of magnetic softness is due to demolition of nanocrystalline structure in the wake of secondary crystallization. An interesting observation in our prior work showed an improvement in magnetic softness at elevated temperatures by only 2 at.% substitution of Ge for Co in $Fe_{44}Co_{44}Zr_7B_5$ (Cu-free Hitperm composition) [10]. We have further found that the small quantity of Ge substitution has an influence on both primary and secondary crystallization temperatures. The similar result was also reported in $Fe_{78}Co_5Zr_6B_{10}Cu_1$ alloy [11]. However, effect of the Ge substitution on crystallization kinetic for the alloy has not been fully understood, which we believe, provides an insight to the underlying microscopic origin behind the above observations.

Since crystallization of amorphous alloys is characterized by phase transition, one can express the transformation rate by $d\alpha/dt = kf$. Here, α and t represent conversion fraction and transformation time, while k is reaction rate constant as a function of temperature T [12,13]. According to Arrhenius equation, $k = A\exp(-E/RT)$, where A, E and R are pre-exponential factor, activation energy and universal gas constant, respectively. It is known that f is too tricky and complex to be determined due to its strong dependence on reaction orders which vary with different solid-state reaction mechanisms [14]. In addition, crystallization processes for an amorphous alloy generally involve nucleation, grain growth and/or impingement and exhibit so-called multiple-step characters [15]. Therefore, conventional model-fitting approach [16–18] that requires specific kinetic model or reaction order is not feasible to obtain virtual kinetic parameters

* Corresponding author.
E-mail address: bixf@buaa.edu.cn (X. Bi).

0925-8388/$ – see front matter © 2010 Elsevier B.V. All rights reserved.
doi:10.1016/j.jallcom.2010.09.107

for a crystallization process. In this respect, an iso-conversional method characterized by model-independence has been summarized by Vyazovkin [19–22]. This approach has proved an effective way in obtaining local activation energies corresponding to different stages of solid-state phase transformations with no need for their respective kinetic models.

The iso-conversional approach was adopted in this work to investigate effect of Ge partial substitutions for Co in $Fe_{44}Co_{44}Zr_7B_5$ alloy on its crystallization kinetics in the frame of extended Kissinger model. Dependence of microstructure and composition distribution on Ge substitutions is studied using scanning transmission electron microscopy and X-ray diffraction analysis. Furthermore, in combination with magnetic property for the annealed $Fe_{44}Co_{44-x}Zr_7B_5Ge_x$, microscopic origin underlying the role of Ge substitutions in thermal stabilization of nanostructure is discussed.

2. Experimental

$Fe_{44}Co_{44-x}Zr_7B_5Ge_x$ (x = 0–4 at.%) ingots were prepared using mixture of Fe (99.9%), Co (99.96%), Zr (99.5%), Ge (99.999%) and FeB chips containing 21 wt.% B by arc-melting in an argon atmosphere. The percentage in parenthesis represents purity. Ribbons of 1 mm-wide and 20 μm-thick were produced from the ingots by conventional melt-spinning technique. Crystallization processes were evaluated by differential scanning calorimetry (DSC) (Netzsch Sta 449C) at heating-rates ranging from 5 to 30 K/min in an argon atmosphere. DSC curves were all calibrated by removing background signals from original measuring curves. Magnetic variations during heating-up processes were evaluated by thermomagnetic gravimetry (TG) under a magnetic field of 10 Oe. Microstructural characterizations were investigated using X-ray diffraction analysis (XRD) for crystalline structure, transmission electron microscopy (TEM) (JEM-2100F) operated at 200 KV for nanocrystal size, selected area electron diffraction (SAED) for minor precipitates and scanning transmission electron microscopy (STEM) (JEM-2100F) for composition distributions of elements. Isothermal annealing was performed in vacuum for 0.3–20 h, and coercivity of the annealed alloys was measured by vibrating sample magnetometer.

3. Results and discussion

3.1. Calorimetric measurements

Fig. 1 displays DSC and TG curves measured at a heating-rate of 20 K/min for the as-spun $Fe_{44}Co_{44-x}Zr_7B_5Ge_x$ alloys. For simplicity, $Fe_{44}Co_{44}Zr_7B_5$, $Fe_{44}Co_{43}Zr_7B_5Ge_1$ . . . and $Fe_{44}Co_{40}Zr_7B_5Ge_4$ are denoted as Ge0, Ge1, . . . and Ge4, respectively. It is seen that all the alloys exhibit two exothermic peaks in the DSC curves within the temperature range in concern. As confirmed by XRD analysis, the peaks stem from formation of FeCo phase and Zr-type phases due to primary and secondary crystallizations, respectively. The primary-crystallized alloys exhibit a typical microstructure characterized by 10 nm FeCo nanocrystals embedded in a residual amorphous phase, as observed by TEM. Moreover, there appear two steps in each TG curve at temperatures corresponding to the crystallization onsets as shown in DSC curves. The initial reduction in magnetization with increasing temperatures results from increasing thermal energy that competes against magnetic exchange interaction of the amorphous phase, while the subsequent rise in the magnetization obviously arises from formation of the FeCo nanocrystalline phase. In addition, magnetization of the alloys shows a slight increase at temperatures where the secondary crystallizations occur, as also observed in Hitperm alloys [1]. It should be noted that the crystallization onsets are strongly dependent on Ge contents. As the Ge contents increase, the primary crystallization onset decreases from 775.9 to 766.7 K, whereas the secondary crystallization onset increases from 968.0 to 1002.6 K. The temperature range over which the two-phase structure exists is consequently broadened with the Ge contents. The extension of the secondary onsets to higher temperatures is beneficial to thermal stability of the two-phase nanostructure, which in turn contributes to magnetic softness at high temperatures.

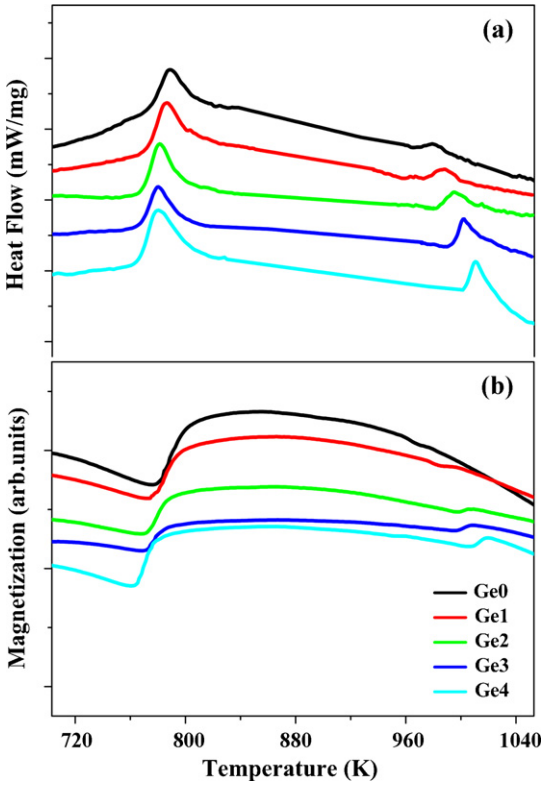

Fig. 1. Calorimetric measurements at a heating-rate of 20 K/min for the as-spun $Fe_{44}Co_{44-x}Zr_7B_5Ge_x$ (x = 0–4 at.%) alloys: (a) DSC and (b) TG curves.

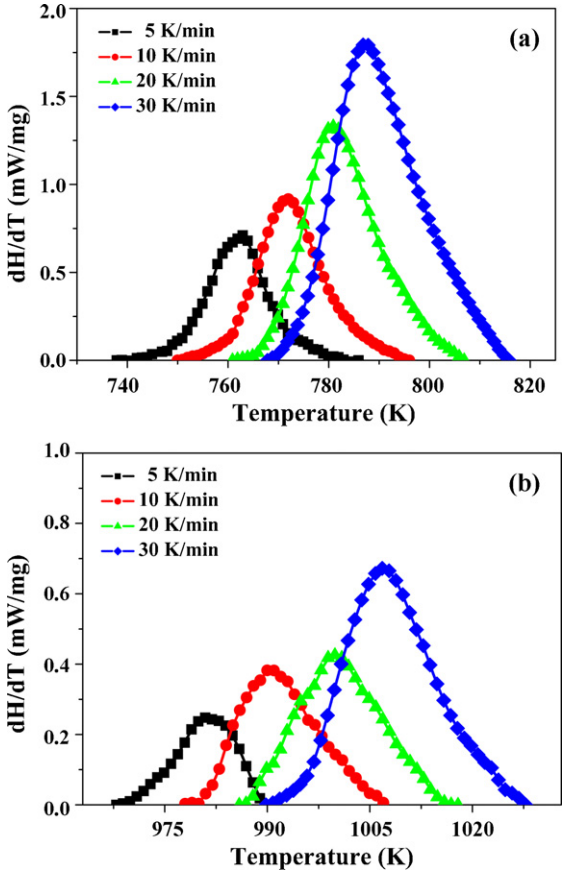

Fig. 2. DSC exothermic peaks attributed to (a) primary and (b) secondary crystallizations for $Fe_{44}Co_{42}Zr_7B_5Ge_2$ alloy, depending on variant heating-rates.

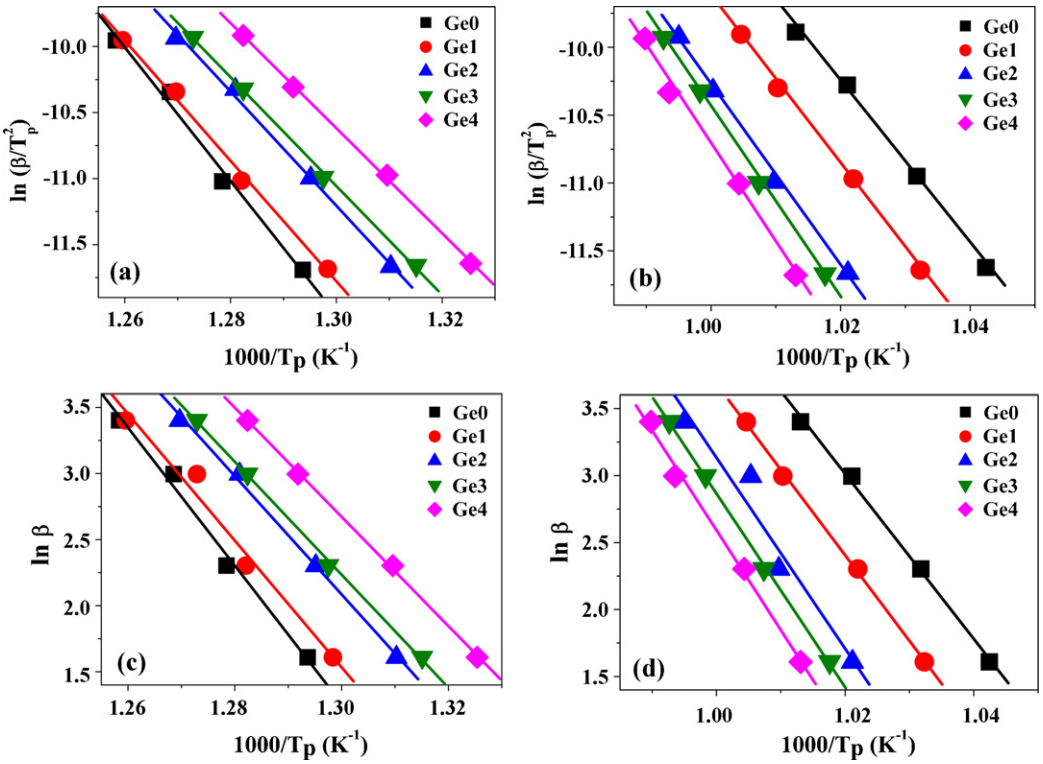

Fig. 3. Kissinger plots of (a) primary (b) secondary crystallizations, and Ozawa plots of (c) primary (d) secondary crystallizations for $Fe_{44}Co_{44-x}Zr_7B_5Ge_x$ (x = 0–4 at.%) alloys.

3.2. Crystallization kinetics

Effect of the partial substitution of Ge on activation energy of the crystallizations has been studied. It is known that, under a non-isothermal condition with a constant heating-rate $\beta = dT/dt$, a transformation rate can be expressed by differential or integral equation [23]. However, reaction function and temperature integral required in the respective expression are too complex to give rise to an analytical solution. In this respect, the Kissinger [24] and Ozawa [25,26] models have been applied with a hypothesis of the maximum transformation rate occurring at peak temperatures (T_p) in DSC curves, $d[df(\alpha)/dt]/dt = 0$. Based on the Kissinger theory, a phase transition can be described by,

$$\ln\left(\frac{\beta}{T_p^2}\right) = -\frac{E_c}{RT_p} + \ln\frac{AR}{E_c} \quad (1)$$

where T_p, β, R, E_c and A represent peak temperatures in DSC curves, heating-rates, gas constant, activation energy and pre-exponential factor (also known as frequency factor), respectively. Fig. 2(a) and (b) display heating-rate dependent DSC curves around peak temperatures, T_p^p and T_p^s, of the primary and secondary crystallizations for $Fe_{44}Co_{42}Zr_7B_5Ge_2$. The crystallization peaks are both shifted to higher temperatures with increasing heating-rates. Similar results are observed in $Fe_{44}Co_{44-x}Zr_7B_5Ge_x$ (x = 0, 1, 3, 4) alloys. Table 1 summarizes the characteristic transition temperatures as a function of the heating-rates for the alloys. As plotted in Fig. 3(a) and (b), the $\ln(\beta/T_p^2) \sim 1/T_p$ reveals a linear relationship for both the primary and the secondary crystallizations. On the other hand, according to Ozawa theory, a phase transition can be described by

$$\ln\beta = -\frac{1.0516E_c}{RT_p} + \ln\frac{AE_c}{R} - 5.330 \quad (2)$$

Fig. 3(c) and (d) illustrate the plots of $\ln\beta$ as a function of $1/T_p$ for the Ge0, Ge1 ... and Ge 4 alloys, showing a linear relationship as well. The E_c values derived from the two models as a function of Ge contents, as summarized in Fig. 4, are in a good agreement. It should be mentioned that the results exhibit the same magnitude of order as those on other FeCo-based amorphous alloys [27–29]. It is also seen that E_c^p of the primary crystallization decreases with increasing the Ge content, whereas E_c^s of the secondary crystallization increases.

Concerning multiple-step character of the crystallization processes, change of activation energy with degree of crystallization should be taken into account to reveal variations of kinetic behavior during the processes [29]. Supposing that mechanism of each step remains unchanged with changing of temperatures, one can approximately regard the crystallization as an iso-conversional transformation [30]. Crystallization fraction, α, is then proportional to the area of exothermic peaks in the DSC curves, which can be given by $\alpha = \Delta H(T)/\Delta H_{total}$, where $\Delta H(T)$ and ΔH_{total} represent partial enthalpy change and total enthalpy change of the whole transformation process, respectively. Fig. 5(a) and (b) demon-

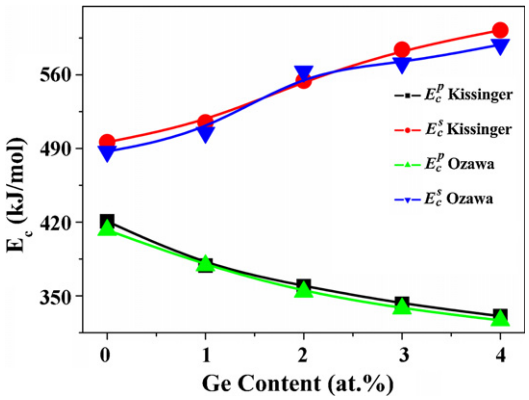

Fig. 4. Effect of the Ge substituted content on activation energy for primary crystallization (E_c^p) and secondary crystallization (E_c^s), which are estimated from Kissinger and Ozawa models, respectively.

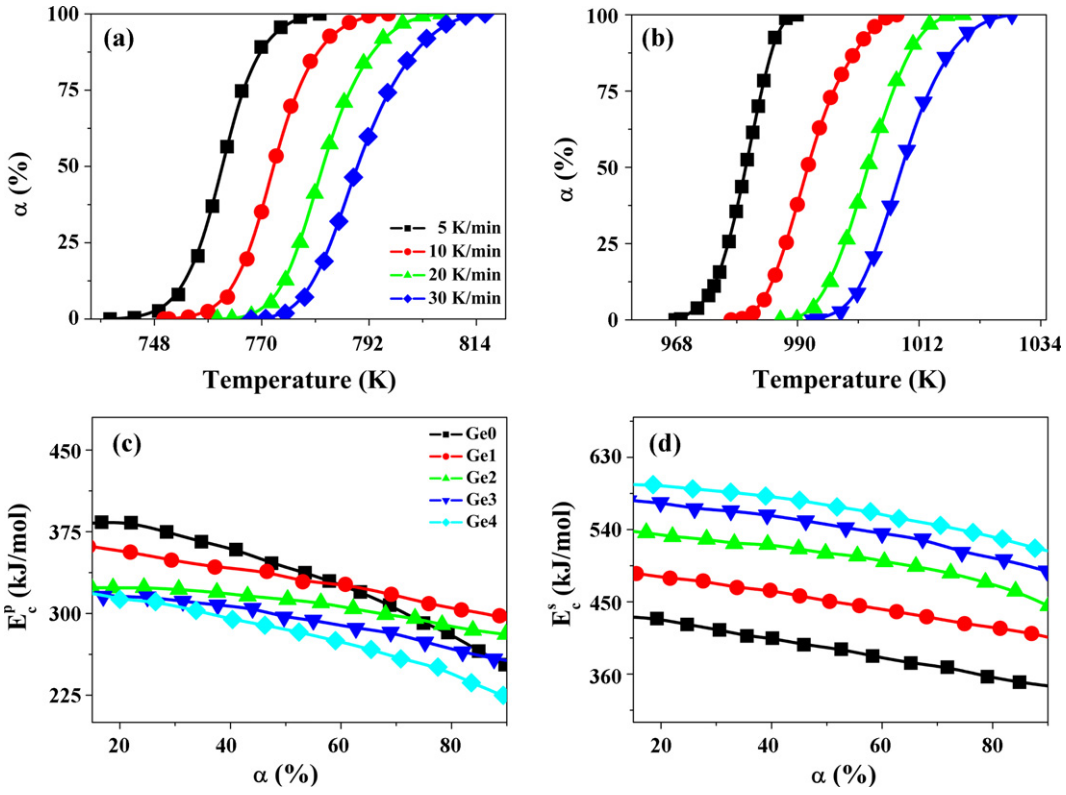

Fig. 5. Curves of α–T for (a) primary and (b) secondary crystallizations for $Fe_{44}Co_{42}Zr_7B_5Ge_2$ alloy; effect of the Ge substituted content on local activation energies of (c) primary and (d) secondary crystallizations as a function of α for the alloys.

strate change of crystallization fraction with temperature for $Fe_{44}Co_{42}Zr_7B_5Ge_2$, as a function of heating-rate. The α–T curves exhibit a sigmoid-type character. Based on generalized Kissinger approach [24,31], local activation energy $E_c(\alpha)$ can be given by

$$\ln\frac{\beta}{T_{\alpha\beta}^2} = -\frac{E_c(\alpha)}{RT_{\alpha\beta}} + \ln\frac{AR}{E_c(\alpha)} + \ln\left[-\frac{df(\alpha)}{d\alpha}\right]_{\alpha_p} \quad (3)$$

where $T_{\alpha\beta}$ determined from DSC curves is the temperature corresponding to crystallization fraction and heating-rate. The α_p is transformation fraction at the peak temperature T_p. Plots of $\ln \beta/T_{\alpha\beta}^2$ verses $1/T_{\alpha\beta}$ have revealed linear relationships for all the alloys. The local activation energy as a function of crystallization fraction is then estimated from the plots. As shown in Fig. 5(c) and (d), the activation energies for the crystallization processes are both reduced with the fractions. The reduction of $E_c(\alpha)$ with α indicates that mixed nucleation including site saturation and continuous nucleation, rather than Avrami nucleation, occurs during the crystallizations [30,32]. It is interesting to find that $E_c^p(\alpha)$ for the primary crystallization tend to decrease with an increase of the Ge substitution, whereas $E_c^s(\alpha)$ for the secondary crystallization shows an increase. It can be suggested that Ge act as heterogeneous nucleation agents in the amorphous precursor, which is probably due to local compositional fluctuations resulting from the introduction of Ge, as proposed for the effect of Cu in FeSi-based alloys [33]. For the secondary crystallization, the increase of activation energy with Ge content indicates that Ge has an effect of hindering the secondary crystallizations, which becomes more pronounced with increasing the Ge content.

Table 1
Exothermic peak temperatures attributed to the primary crystallization (T_p^p) and secondary crystallization (T_p^s) for $Fe_{44}Co_{44-x}Zr_7B_5Ge_x$ (x = 0–4 at.%) alloys as a function of heating-rates during DSC measurements.

$Fe_{44}Co_{44-x}Zr_7B_5Ge_x$	Peak temperature of primary crystallization T_p^p (K)			
X	5 K/min	10 K/min	20 K/min	30 K/min
0	773.0	782.2	788.3	794.7
1	770.2	780.0	787.6	793.9
2	763.2	772.1	780.7	787.6
3	760.4	770.7	779.8	785.6
4	754.5	682.6	774.1	779.8

	Peak temperature of secondary crystallization T_p^s (K)			
	5 K/min	10 K/min	20 K/min	30 K/min
0	959.3	969.2	979.4	987.1
1	968.7	978.5	989.8	995.4
2	979.3	990.4	999.7	1005.0
3	982.7	992.7	1001.7	1007.4
4	987.1	995.7	1006.5	1010.3

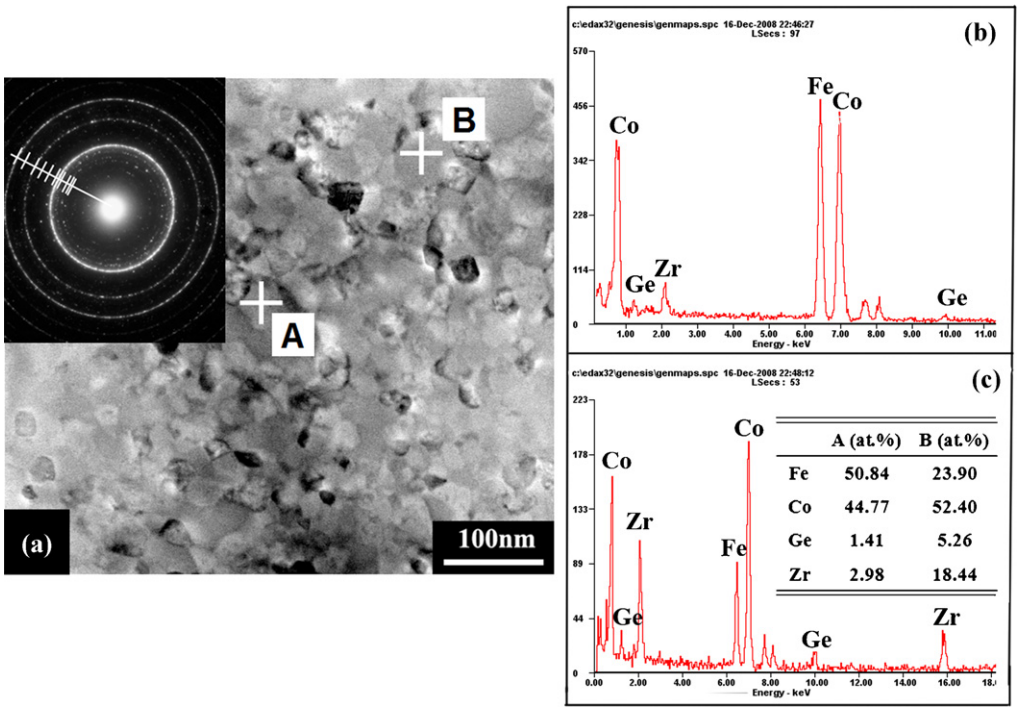

Fig. 6. (a) STEM image of the $Fe_{44}Co_{42}Zr_7B_5Ge_2$ alloy annealed at 973 K for 1 h along with SAED pattern (inserted). From centre to edge, the rings and spots (their positions are marked with bars) correspond to (4 0 0), (3 3 1), (4 2 2), (5 1 1) of $(FeCo)_3Zr$, (1 1 0) of α/α'-(FeCo), (4 4 0), (6 2 2), (5 5 1) of $(FeCo)_3Zr$, (2 0 0) of α/α'-(FeCo), (5 5 5) of $(FeCo)_3Zr$ and α/α'-(FeCo) (2 1 1), respectively; (b) and (c) are EDS spectra for the two areas marked as "A" and "B", respectively.

3.3. Compositional distributions

In order to clarify microscopic origins responsible for the enhanced thermal stability of two-phase nanocrystalline structure due to the partial substitution of Ge, distribution of elements needs to be analyzed. Up to date, atom probe field ion microscopy (APFIM) and three-dimensional atom probe technique (3DAP) have been applied to understand the role of Cu in the observed nanocrystalline microstructure of FeSi-based and FeCo-based alloys, respectively. The 3DAP analysis along with TEM reveals that Cu is unnecessary for FeCo-based alloys to form a nanocrystalline microstructure [34,35]. In this work, to understand the role of Ge in FeCo-based alloys, STEM observations along with EDS analysis were made for the $Fe_{44}Co_{42}Zr_7B_5Ge_2$ annealed at 973 K (higher than the secondary crystallization onset of the alloy). As shown in the inset of Fig. 6(a), several distinct spots identified as Zr-type phase are observed near diffraction rings stemming from FeCo phase. In addition, the alloy exhibits large grains with irregular shape. Composition analysis was further made for two typical areas labeled as "A" and "B", respectively, as shown in Fig. 6(b) and (c). It should be noted that the copper peak is caused by copper clamps and those appearing at low energy side caused by carbon. It is seen that area "A" exhibits smaller intensities of the peaks indexed as Ge, Zr and Co, respectively, as compared to area "B". The relative quantities of Ge, Zr, Co and Fe estimated from the peak intensities are listed in the inset of Fig. 6(c). As can be seen, Co/Fe ratio in area "A" is close to unity, while Zr and Ge contents are much lower compared to those in area "B". By contrast, area "B" exhibits Co/Fe ratio of about 2:1 and higher contents of Zr and Ge. It is evident that the alloy consists of FeCo crystalline (area "A") and residual amorphous phase (area "B") prior to the secondary crystallization. The large content of Co existing in the residual amorphous phase also explains the fact that Curie temperature of the amorphous phase is higher than those of Fe or FeSi-based nanocrystalline alloys. The characteristic of compositional distribution indicates that Ge has a tendency of partitioning in the residual amorphous phase which is enriched with Zr and B. The argument is supported from thermodynamic data: Ge has large negative enthalpy when mixed with Zr and Co [35–37]. On the other hand, it is generally believed that partitioning layers of early transition metals are formed across the interface between nanocrystalline and amorphous phase due to slow diffusion of the atoms into interior of the residual amorphous phase caused by their large atomic radii [38]. The Zr-partitioning layer acts as a diffusion barrier against grain growth of the FeCo phase and consequently stabilize the two-phase nanostructure [8,39]. However, as Zr continues to pile up to a critical content, secondary crystallization is eventually induced during which the Zr-type phase is crystallized from the residual amorphous phase, leading to grain growth of FeCo phase. Evidently, the partitioning of Ge in the residual amorphous phase benefits stabilization of the diffusion barrier, which reflects extension of the secondary crystallization onset to higher temperatures. Coercivity and microstructures for the annealed alloys have been shown to be consistent with the stabilization effect of Ge.

3.4. Coercivity and microstructures

Fig. 7 shows changes of coercivity with various annealing parameters. In the temperature range of 723–873 K, coercivity remains about 1 Oe for the $Fe_{44}Co_{44}Zr_7B_5$ and $Fe_{44}Co_{42}Zr_7B_5Ge_2$ annealed up to 10 h. A clear difference in the coercivity for the two alloys is observed when annealed at 923 K. The $Fe_{44}Co_{44}Zr_7B_5$ without Ge substitution exhibits a dramatic increase in the coercivity from 1 to 20 Oe when annealed for 5 h. As the annealing holds up to 10 h at 923 K, the Ge-substituted alloy remains smaller coercivity as compared to $Fe_{44}Co_{44}Zr_7B_5$. Microstructure of the annealed alloys was investigated by TEM observations. As shown in Fig. 8(a) and (b), it reveals similar microstructures for the two alloys annealed at 923 K for 1 h, characterized by FeCo nanocrystallites of about 10 nm embedded in a residual amorphous matrix. With the annealing time increasing up to 10 h, however, the $Fe_{44}Co_{44}Zr_7B_5$ alloy displays a larger grain size with respect to $Fe_{44}Co_{42}Zr_7B_5Ge_2$ (Fig. 8(c) and (d)). In addition, a few additional but weak spots adjacent to

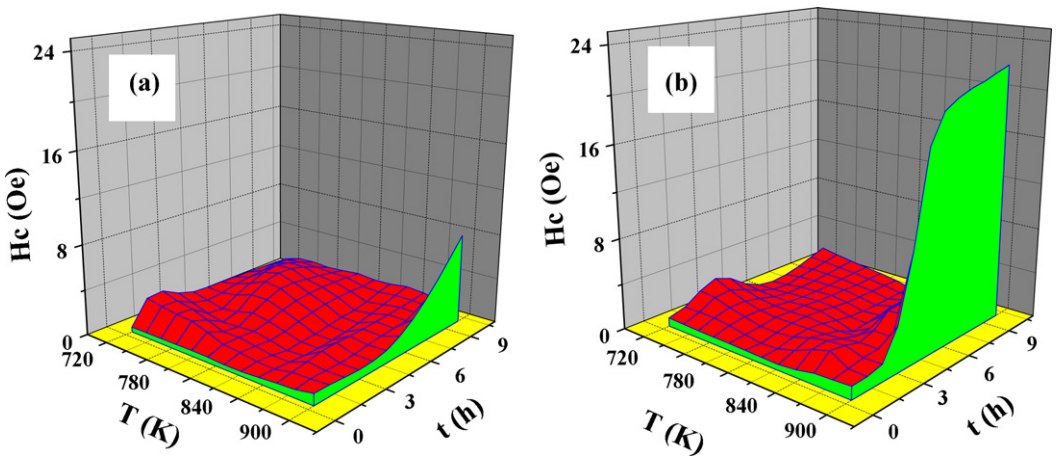

Fig. 7. Dependence of coercivity on annealing temperature and time for (a) $Fe_{44}Co_{42}Zr_7B_5Ge_2$ and (b) $Fe_{44}Co_{44}Zr_7B_5$ alloys, respectively.

(1 1 0) diffraction rings (marked as green circles) are observed in the SAED patterns for the $Fe_{44}Co_{44}Zr_7B_5$ alloy, which arise from formation of Zr-type phase identified as (5 1 1), (5 5 1) and (5 5 5) of $(FeCo)_3Zr$ phase [8]. By contrast, the precipitates are not detected in $Fe_{44}Co_{42}Zr_7B_5Ge_2$ within the sensitivity of electron diffraction analysis. Obviously, grain growth occurs in the wake of the precipitation of the Zr-type phase. Furthermore, we have investigated change of coercivity for the alloys annealed at different temperatures for up to 20 h. The results are listed in Table 2. It is seen that coercivity starts to increase for the Ge-free alloy annealed at 883 K and exhibits a coercivity of 31 Oe at 903K. By contrast, coercivity of the $Fe_{44}Co_{42}Zr_7B_5Ge_2$ remains low value of 1.68 Oe after annealed at the same temperature, which is evidently attributed to the role of Ge substitution in retarding the secondary crystallization. It is noticed that the secondary crystallization temperatures derived from the variations of coercivity is lower than the crystallization

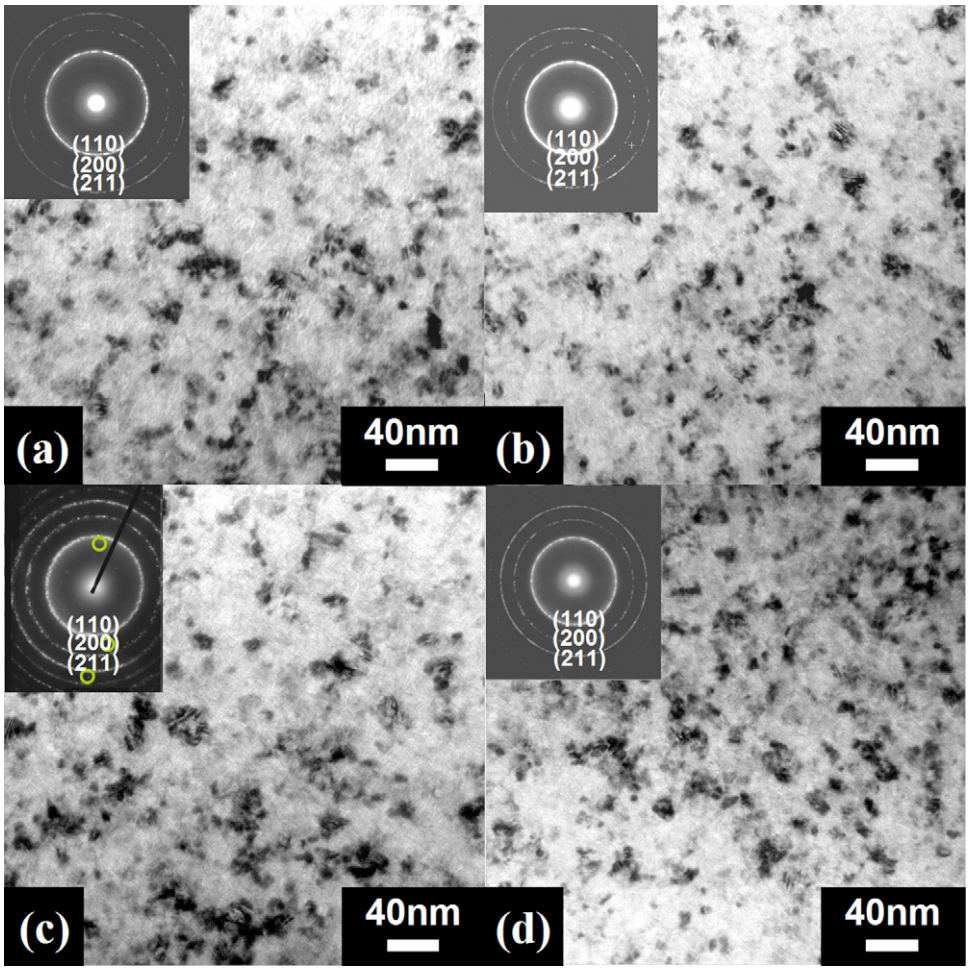

Fig. 8. TEM images and corresponding SAED patterns for the alloys annealed at 923 K: (a) and (c) for the $Fe_{44}Co_{44}Zr_7B_5$ annealed for 1 and 10 h, respectively; (b) and (d) for $Fe_{44}Co_{42}Zr_7B_5Ge_2$ annealed for 1 and 10 h, respectively.

Table 2
Coercivity of $Fe_{44}Co_{44}Zr_7B_5$ and $Fe_{44}Co_{42}Zr_7B_5Ge_2$ alloys annealed at different temperatures for 20 h.

Annealed temperature (K)	H_c (Oe)	
	$Fe_{44}Co_{44}Z_7B_5$	$Fe_{44}Co_{42}Zr_7B_5Ge_2$
923	45.45	54.96
913	36.90	18.27
903	31.01	1.68
893	3.16	1.59
883	2.58	1.33
873	1.30	1.25

onsets measured from the DSC curves, which can be explained by the fact that crystallization is a diffusion-controlling process.

4. Conclusions

We have studied primary and secondary crystallization processes for $Fe_{44}Co_{44}Zr_7B_5$ alloys with partial substitution of Ge for Co by performing a series of non-isothermal processes at variant heating-rates. Detailed kinetic analysis has been made by applying mechanism-independent iso-conversional approach in the framework of extended-Kissinger model. It is observed that the Ge substitution facilitates the primary crystallization by reducing its activation energy for $Fe_{44}Co_{44}Zr_7B_5$. In particular, the presence of Ge is found to enhance thermal stability of two-phase nanocrystalline structure by increasing activation energy of the secondary crystallization. The peculiar effect of Ge on the crystallizations becomes more pronounced with increasing the Ge substitution content. The results are suggested to be attributed to the retention of Ge in residual amorphous phase, which retards occurrence of the secondary crystallizations. Variations of microstructure and coercivity with the Ge substitution exhibit that the Ge-substituted alloys remain small coercivity even after long-time annealing above 873 K.

Acknowledgment

This work is supported by the Science Fund for Creative Research Groups (50921003).

References

[1] M.A. Willard, D.E. Laughlin, M.E. McHenry, D. Thoma, K. Sickafus, J.O. Cross, V.G. Harris, J. Appl. Phys. 84 (1998) 6773.
[2] M.A. Willard, M.-Q. Huang, D.E. Laughlin, M.E. McHenry, J.O. Cross, V.G. Harris, C. Franchetti, J. Appl. Phys. 85 (1999) 4421.
[3] K. Suzuki, J.M. Cadogan, Phys. Rev. B 58 (1998) 2730.
[4] A. Hernando, M. Vazquez, T. Kulik, C. Prados, Phys. Rev. B 51 (1995) 3581.
[5] G. Herzer, IEEE Trans. Magn. 25 (1989) 3327.
[6] G. Herzer, IEEE Trans. Magn. 26 (1990) 1397.
[7] G. Herzer, Scr. Metall. Mater. 33 (1995) 1741.
[8] H.F. Li, D.E. Laughlin, R.V. Ramanujan, Philo. Mag. 86 (2006) 1355.
[9] X.B. Liang, J. Ferenc, T. Kulik, B. Xu, Mater. Sci. Eng. A 426 (2006) 169.
[10] Y. Sun, L. Zhong, X.F. Bi, Scr. Mater. 60 (2009) 814.
[11] J.S. Blazquez, S. Roth, A. Conde, J. Alloy Compd. 395 (2005) 313.
[12] G.N. Lewis, Z. Phys. Chem. 52 (1905) 310.
[13] M.L. Bruner, S. Tolloczko, Z. Anorg, Allg. Chem. 56 (1908) 58.
[14] S. Vyazovkin, Thermochim. Acta 211 (1992) 181.
[15] S. Vyazovkin, Int. Rev. Phys. Chem. 19 (2000) 45.
[16] M.E. Brown, Reaction in the Solid-state, Elsevier, Amsterdam, 1980.
[17] J. Sestak, Thermophysical Properties of solids, Elsevier, Amsterdam, 1984.
[18] A.K. Galwey, M.E. Brown, Thermal Decomposition of Ionic Solid, Elsevier, Amsterdam, 1999.
[19] S. Vyazovkin, J. Therm. Anal. Calorim. 83 (2006) 45.
[20] S. Vyazovkin, C.A. Wight, Int. Rev. Phys. Chem. 17 (1998) 407.
[21] S. Vyazovkin, N. Sbirrazzuoli, J. Therm. Anal. Calorim. 72 (2003) 681.
[22] S. Vyazovkin, Thermochim. Acta 355 (2000) 155.
[23] A. Ortega, Thermochim. Acta 284 (1996) 379.
[24] H.E. Kissinger, Anal. Chem. 29 (1957) 1702.
[25] T. Ozawa, J. Therm. Anal. 2 (1970) 301.
[26] T. Ozawa, Polymer 12 (1971) 150.
[27] Z.Z. Yuan, X.D. Chen, B.X. Wang, Z.J. Chen, J. Alloy Compd. 399 (2005) 166.
[28] B. Majumdar, S. Bysak, D. Akhtar, J. Magn. Magn. Mater. 309 (2007) 300.
[29] J.S. Blazquez, C.F. Conde, A. Conde, Acta Mater. 53 (2005) 2305.
[30] F. Liu, S.J. Song, J.F. Xu, J. Wang, Acta Mater. 56 (2008) 6003.
[31] N.S. Fatemi, R. Whitehead, D. Price, D. Dollimore, Thermochim. Acta 78 (1984) 437.
[32] A.T.W. Kempen, F. Sommer, E.J. Mittemeijer, J. Mater. Sci. 37 (2002) 1321.
[33] K. Hono, D.H. Ping, M. Ohnuma, H. Onodera, Acta Mater. 47 (1999) 997.
[34] M. Ohnuma, D.H. Ping, T. Abe, H. Onodera, K. Hono, J. Appl. Phys. 93 (2003) 9186.
[35] D.H. Ping, Y.Q. Wu, K. Hono, M.A. Willard, M.E. McHenry, D.E. Laughlin, Scr. Mater. 45 (2001) 781.
[36] K. Suzuki, J.W. Cochrane, J.M. Cadogan, X.Y. Xiong, K. Hono, J. Appl. Phys. 91 (2002) 8417.
[37] J.S. Blazquez, S. Roth, C. Mickel, A. Conde, Acta Mater. 53 (2005) 1241.
[38] P.R. Ohodnicki Jr., Y.L. Qin, D.E. Laughlin, M.E. McHenry, M. Kodzuka, T. Ohkubo, K. Hono, M.A. Willard, Acta Mater. 57 (2009) 87.
[39] R. Goswami, M.A. Willard, Scr. Mater. 59 (2008) 459.